Numerical studies of a plasma diode with external forcing

V. L. Rekaa, H. L. Pécseli, and J. K. Trulsen

Citation: Physics of Plasmas **19**, 082115 (2012); doi: 10.1063/1.4747620
View online: http://dx.doi.org/10.1063/1.4747620
View Table of Contents: http://aip.scitation.org/toc/php/19/8
Published by the American Institute of Physics

Numerical studies of a plasma diode with external forcing

V. L. Rekaa,[1,a)] H. L. Pécseli,[1,b)] and J. K. Trulsen[2,c)]
[1]Department of Physics, University of Oslo, Box 1048 Blindern, N-0316 Oslo, Norway
[2]Institute of Theoretical Astrophysics, University of Oslo, Box 1029 Blindern, N-0315 Oslo, Norway

(Received 30 March 2012; accepted 7 August 2012; published online 23 August 2012)

With reference to laboratory Q-machine studies we analyze the dynamics of a plasma diode under external forcing. Assuming a strong axial magnetic field, the problem is analyzed in one spatial dimension by a particle-in-cell code. The cathode is assumed to be operated in electron rich conditions, supplying an abundance of electrons. We compare different forcing schemes with the results obtained by solving the van der Pol equation. In one method of forcing we apply an oscillation in addition to the DC end plate bias and consider both amplitude and frequency variations. An alternative method of perturbation consists of modelling an absorbing grid at some internal position. Also in this case we can have a constant frequency with varying amplitude or alternatively an oscillation with chirped frequency but constant amplitude. We find that the overall features of the forced van der Pol equation are recovered, but the details in the plasma response need more attention to the harmonic responses, requiring extensions of the model equation. The analysis is extended by introducing collisional effects, where we emphasize charge exchange collisions of ions, since these processes usually have the largest cross sections and give significant modifications of the diode performance. In particular we find a reduction in oscillator frequency, although a linear scaling of the oscillation time with the system length remains also in this case. © *2012 American Institute of Physics*. [http://dx.doi.org/10.1063/1.4747620]

I. INTRODUCTION

The present paper discusses the performance of a long plasma diode of length $\mathcal{L}$ as studied by numerical methods. The basic model corresponds to a single ended Q-machine,[1,2] where electrons are emitted thermally while ions are produced by surface ionization at a hot cathode. In the basic version of the Q-machine the ions are produced by contact ionization[3] of hot alkali metals with suitable work functions.[4] The metal plate also supplies electrons by Richardson emission. We will in the following assume that a confining axial magnetic field is sufficiently strong to justify a description in one spatial dimension. This configuration has been studied extensively for instance to find steady state potential variations, some involving trapped plasma populations or "virtual cathodes."[5–7] For weaker magnetic fields the dynamics are changed since the particles are no longer confined to move along the magnetic field lines.[8] Our analysis emphasizes results relevant for Q-machines where $\mathcal{L}/\lambda_{De} > \sqrt{M/m}$ in terms of the Debye length λ_{De} and the electron-ion mass ratio M/m, but the basic principles have more general applications, for instance for diodes.[9,10] Diodes as well as Q-machines can be operated in electron rich or ion rich conditions, depending on the relative abundance of the two species emitted at the surface. The present study assumes electron rich conditions which are also the most common one for Q-machine applications.

The performance of an oscillating diode with a cold positively biased end plate is usually modelled by a van der Pol equation.[11–13] The present study will address the accuracy of the van der Pol model for describing the diode for unstable conditions. For a freely oscillating diode, the conditions are well defined. In the case of external forcing, also included in the van der Pol model, the situation is ambiguous: it is not obvious how to apply perturbations to a physical diode. Several methods will be discussed and compared here. The basic diagnostics of the diode performance will be the fluctuating current through the diode.

Several studies discuss chaotic behaviour of diodes,[14,15] but these topics will not be addressed here. Also, non-neutral diodes have been studied elsewhere.[16–19]

II. STANDARD CONDITIONS

Under standard operating conditions for a Q-machine, we have electron rich conditions, where the hot plate at $x = 0$ can supply electrons in abundance. The electrons are emitted with a velocity distribution $n_{0e}\sqrt{2m/\pi T_0}\exp(-\frac{1}{2}mu^2/T_0)$ for $u > 0$, where T_0 is the hot plate temperature in energy units, and similarly for ions we have $n_{0i}\sqrt{2M/\pi T_0}$ $\exp(-\frac{1}{2}Mu^2/T_0)$, where we assume $n_{0e} > n_{0i}$. The distribution functions are normalized over the interval $u \in \{0; \infty\}$. Our reference case corresponds to electron rich conditions with $n_{0e}/n_{0i} = 2$. For such cases, the plasma assumes a negative potential in front of the cathode in order to reflect the surplus of electrons, while ions on the other hand are accelerated by the potential drop. The numerical plasma injection scheme used here differs from the one used in some other related studies.[20]

With standard operation, the cold end plate at $x = \mathcal{L}$ is biased negatively at a potential $-\Psi$, reflecting most of the electrons: only the most energetic tail of the Maxwellian velocity distribution has sufficient energy to overcome the

a)Electronic mail: v.l.rekaa@fys.uio.no.
b)Electronic mail: hans.pecseli@fys.uio.no.
c)Electronic mail: jan.trulsen@astro.uio.no.

reflecting potential, while all ions will be absorbed at the end plate. For long systems we have conditions where the plasma is quasi-neutral and has a large region at an approximately constant potential, the plasma potential $-\Phi_p$. The plasma is not in thermal equilibrium and for $x > 0$ it has no characteristic temperature. A useful length-measure will here be the Debye length defined in terms of the reference temperature T_0. Similarly we can define a reference ion sound speed by the same temperature. For conditions relevant for the present study, the plasma density will be inhomogeneous and non-stationary. To have an unambiguous definition of a Debye length we use n_{0e} for the density.

We first assume the axially varying potential to be negative, $-\Phi(x)$ with $\Phi(x) > 0$, for all x. For the ion density we have the consistency relation

$$n_i(x) = n_{0i} \exp(e\Phi/T_0)(1 - \mathrm{erf}\sqrt{e\Phi/T_0}), \quad (1)$$

with erf being the error function. For the electrons we have

$$n_e(x) = n_{0e} \exp(-e\Phi/T_0)\left(1 + \mathrm{erf}\sqrt{e(\Psi - \Phi)/T_0}\right), \quad (2)$$

as long as the end plate potential is below the plasma potential in the device, $\Psi > \Phi_p > 0$. For given T_0, n_{0e}, n_{0i}, and Ψ, the plasma potential Φ_p is found by setting $n_e = n_i$. For varying Ψ, the resulting equation is solved most easily by graphical methods. No solution with a quasi-neutral plateau exists for small Ψ (more precisely, for $n_{0e}/n_{0i} = 2$ and a range $-1.73 < e\Psi/T_0 < 0.2$, no solution with a quasi-neutral plateau exists. This domain corresponds to oscillatory solutions). For a very negative end plate bias $\Psi \to \infty$ with $\mathrm{erf}\sqrt{e(\Psi - \Phi)/T_0} \to 1$, where all electrons are reflected at $x = \mathcal{L}$, the plasma potential is determined as the solution of $\exp(2e\Phi_p/T_0)(1 - \mathrm{erf}\sqrt{e\Phi_p/T_0}) = 2n_{0e}/n_{0i}$, giving for instance $e\Phi_p/T_0 \approx 2.57$ for $n_{0e}/n_{0i} = 2$. Plasma potentials observed in Q-machines[1] are of this order of magnitude. The mass ratio does not enter the result, and only the density ratio n_{0e}/n_{0i} is important, not the individual densities. As long as the end plate is negative compared to the plasma potential, $|\Psi| > |\Phi_p|$, we have the ion current contribution to be constant and equal to the ion flux at the hot plate, $en_{0i}\sqrt{2T_0/M\pi}$. The electron current $en_{0e}\sqrt{2T_0/m\pi}\exp(-e\Psi/T_0)$, on the other hand, changes due to the change in electrons absorbed at the end plate when Ψ is varied.

The average ion velocity at any position x is given by

$$U_i = \sqrt{\frac{2T_0}{\pi M}}\frac{n_{0i}}{n_i(x)} = \sqrt{\frac{2T_0}{\pi M}}\frac{\exp(-e\Phi(x)/T_0)}{1 - \mathrm{erf}\sqrt{e\Phi(x)/T_0}}, \quad (3)$$

using Eq. (1). Defining the edge of the end plate sheath as the position where we have quasi-neutrality, $n_i = n_e$, we can determine the average velocity of the ions as they arrive at the sheath edge for varying bias Ψ. For our reference case with $n_{0e}/n_{0i} = 2$ we find graphically that $U_i \geq 1.8\sqrt{T_0/M}$ for all values of Ψ that allow solutions for a steady state plasma potential Φ_p. A sound speed for the present conditions cannot be defined uniquely, since in general neither ions nor electrons are in thermal equilibrium, but if we use $C_s \approx \sqrt{T_0/M}$ as an estimate, we can argue that the Bohm condition[21,22] is fulfilled with a good margin also in the present case. For the present conditions, the ion accelerating pre-sheath is found at the cathode. Here the pre-sheath is not quasi-neutral as usually assumed.[22]

As long as the end plate bias is below the plasma potential, $|\Phi_p| < |\Psi|$, we have a monotonically decreasing potential $\Phi(x)$, giving a one-to-one correspondence between potential and the axial x-position. Plotting the density difference $n_i - n_e$ as a function of Φ we find that $n_e > n_i$ for all $|\Phi| < |\Phi_p|$, while $n_e < n_i$ for all $|\Phi| > |\Phi_p|$. If we insert the charge density $e(n_i - n_e)$ with Eqs. (1) and (2) into Poisson's equation we conclude (even without solving for $\Phi(x)$) that the curvature of the potential variation $d^2\Phi(x)/dx^2$ is consistent with an electron rich sheath at $x \approx 0$ and an ion rich sheath at $x \approx \mathcal{L}$.

When the end plate potential is changed to be less negative, more electrons will be absorbed at $x = \mathcal{L}$, while all ions will still be absorbed. Eventually the plasma potential and end plate potential become equal. As the end plate potential is made even less negative, the curvature $d^2\Phi(x)/dx^2$ should change to give an electron rich sheath. Since all particles originate from the cathode at $x = 0$, the only way more electrons can arrive at $x \approx \mathcal{L}$ is by changing the plasma potential to be less negative, so that less electrons are reflected by the sheath at $x \approx 0$. From then on the plasma potential will follow the end plate bias as $\Psi \to 0$. At some critical potential it is no longer possible to supply enough electrons and the sheath at the end plate becomes unstable. It is the dynamics of these unstable conditions we study in this work. The origin of the oscillations is often termed the "potential relaxation" instability.[23,24]

Particular attention is here given to the diode response to external perturbations when its end plate is biased positively with conditions that give spontaneously excited oscillations. The results are compared to predictions obtained by the standard van der Pol equation[11,12] that is often used to model this type of diodes. It is demonstrated that this model can account for the free oscillations, while only qualitative agreement is found for the driven cases. Several methods for introducing perturbations of the diode were considered.

Our particle-in-cell (PIC) code is standard,[25] with one important feature being the freedom to impose conditions at the ends of the system, allowing for both Dirichlet and von Neumann conditions. The code allows for introducing collisional effects also. We use the mass ratio for electrons and Hydrogen ions, $M/m = 1836$ and approximately 10^6 particles of each species. The assumed mass ratio can only be considered as representative: a Q-machine, for instance, is usually operated with low ionisation potentials alkali metals, resulting in larger mass ratios. Some early numerical study of diode performance[26] assumed ion to electron mass ratios $M/m \leq 128$, and 3×10^3 particles altogether. Later studies[13] were content with $M/m = 10$, arguing that not much additional knowledge is gained by use of larger M/m-values.

III. PLASMA CONDITIONS WITH VARYING BASIC PARAMETERS

For computational reasons we restrict the length of the system to be $\mathcal{L} = 10^3\lambda_{De}$, noting that we by this choice have

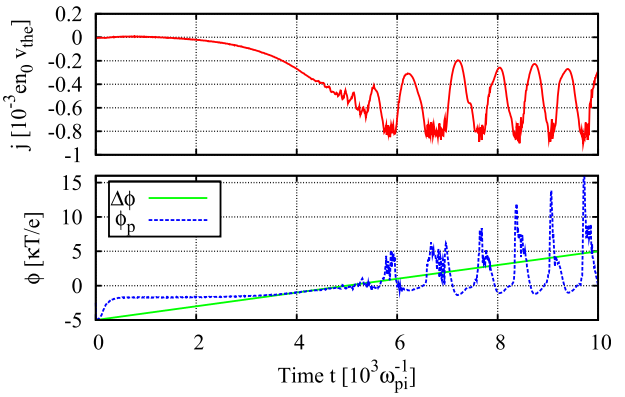

FIG. 1. Variation of the current through the diode (top) and plasma potential at $x = \mathcal{L}/2$ (bottom) for varying end plate bias. Also the externally applied potential sweep at the end plate is shown. The initial current is vanishing since we start with an empty diode.

$\mathcal{L} \gg \lambda_{De}\sqrt{M/m}$ in the reference cases studied. In all cases we initiate the plasma column so that the electrons and ions from the cathode are injected into empty space at $t = 0$. For the given initial condition, the plasma current contains a transient initial part. As an interesting feature we note that very early in the process some of the ions are accelerated to very high velocities, up to 20% of the electron thermal velocity, although the density of these ions is very low.[27] At a later stage, the ions are accelerated by the potential drop at the cathode sheath, and here the velocities are only of the order of $\sqrt{T_0/M}$. The initial acceleration is seen best in a video representation.

To illustrate the basic operating conditions of the plasma diode, we show in Fig. 1 the variations in diode current and plasma potential at $x = \mathcal{L}/2$ as the end plate potential is swept from a large negative to a large positive bias. As long as $-\Psi$ is negative we find a slow change in the current, but at a well defined threshold value, here at $\Psi \approx 0$, we find a sudden onset of low frequency oscillations. The variations in plasma potential and current follow each other, so in the following we use the diode current as the sole diagnostic for the diode performance. Details of the phase space dynamics of ions as well as electrons can be seen in Video 1 (see summary in Fig. 2). During the time interval when $-1 < e\Psi/T_0 < 1$, we find the onset of an instability with wave-length $\lambda \approx \frac{1}{4}\mathcal{L}$, with characteristics different from the saturated diode oscillations. These spontaneously excited, short wavelength, oscillations are assumed to be caused by the ion-electron two stream instability. These oscillations are found only for a narrow interval of the end plate bias.

As long as the end plate potential is sufficiently negative to reflect the majority of the electrons, we find a stable negative plasma potential Φ_p. As the end plate potential $-\Psi$ is made less negative we reach the condition where $|\Psi| = |\Phi_p|$, and from this stage the plasma potential is following Ψ until $\Psi \approx 0$. At this point the sheath becomes unstable, and large

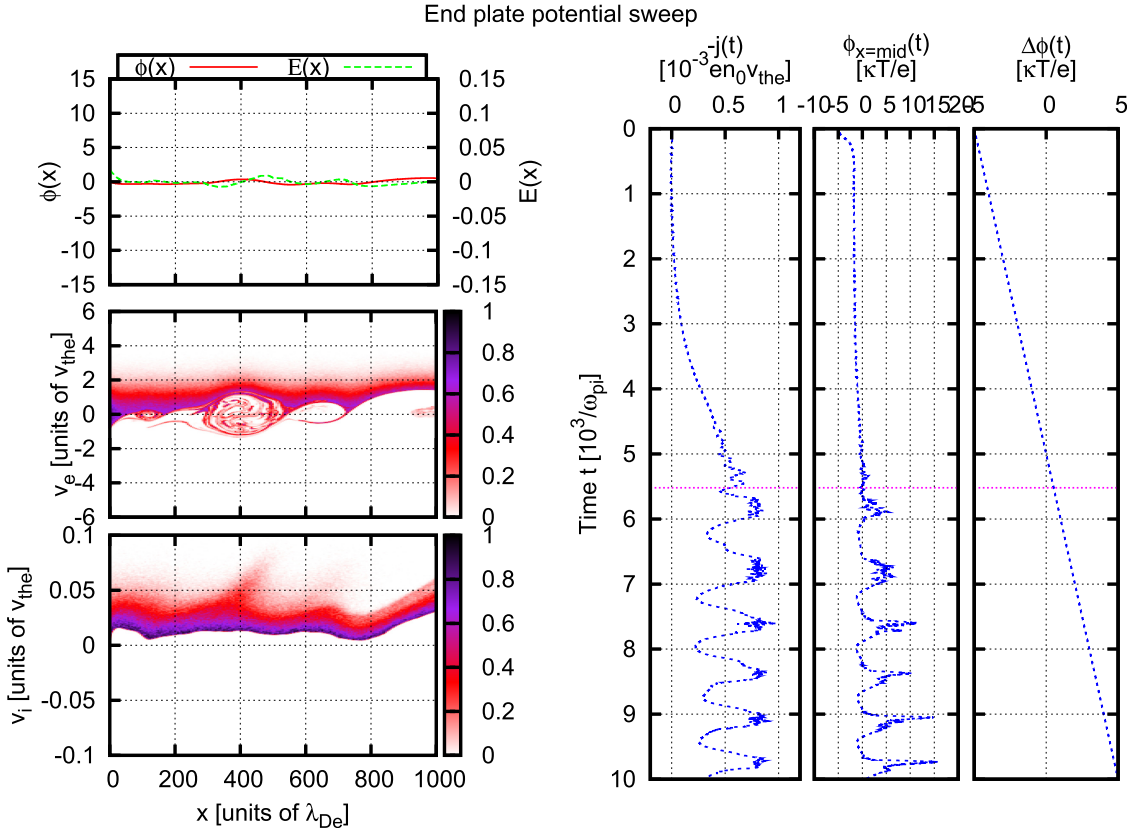

FIG. 2. Summary figure for Video 1, showing also the phase space dynamics. The column to the left shows from the top the potential and electric fields as a function of position. Below we find first the electron phase space and then at the bottom, the ion phase space. The triple column on the right hand side shows the net plasma current (left) and the applied signal (right) with time increasing from top to bottom. The middle panel shows the plasma potential at a position $x = \mathcal{L}/2$. A moving dotted horizontal line gives the time during the video. The frames to the left are obtained at the time indicated by a horizontal dotted line on the right hand side (enhanced online) [URL: http://dx.doi.org/10.1063/1.4747620.1].

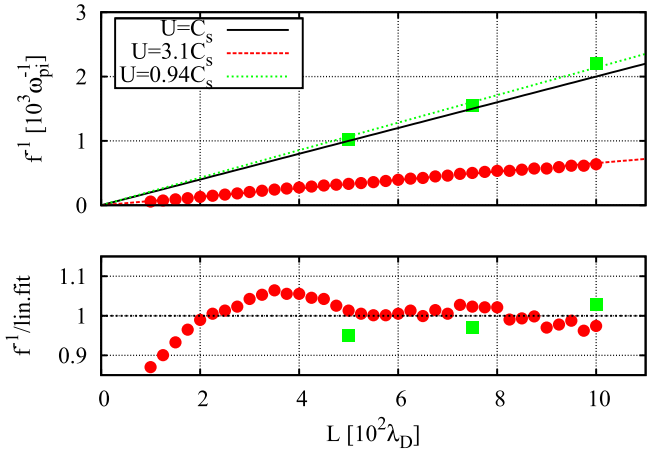

FIG. 3. Illustration of the period of the oscillation of the diode at a large positive bias for varying length of the system $\mathcal{L}$ shown in the top frame with filled red circles. The full line gives $2\mathcal{L}/C_s$ as reference. In the bottom frame we divided the observed normalized oscillation period by the best linear fit to the data in the top frame. With filled green squares we give selected results where the ions undergo change exchange collisions, as explained in Sec. VI.

amplitude, low frequency oscillations are excited (see also Fig. 1). Once the system is unstable, its basic oscillation frequency and saturated amplitude is found to be independent of further increases in the end plate potential, indicating a saturation. The basic oscillation frequency of the oscillations is inversely proportional to the length of the system, as illustrated in Fig. 3. This scaling could invite an interpretation of the instability as a current driven ion acoustic mode,[28] where the most unstable frequency could be assumed to be $f_a \approx C_s/2\mathcal{L}$. If we introduce the standard definition $C_s = \sqrt{T_0/M}$, we find that the observed frequency is approximately 3 times larger than f_a. The simulation allows parameter variations to be obtained with an accuracy much better than what is found in a laboratory. We note that for $\mathcal{L} < 500\lambda_{De}$ there are small but measurable and systematic deviations from this simple proportionality between f_0^{-1} and $\mathcal{L}$. For very short systems, $\mathcal{L} < 80\lambda_{De}$, the oscillations disappear. We attribute this feature to be associated with an overlap of the electron and ion rich sheaths at $x \approx 0$ and $x \approx \mathcal{L}$, respectively.

The details of the phase space dynamics are best seen in Video 1 (Fig. 2). In Fig. 4 we show a sample of phase space for a selected time when the end plate is kept on a constant positive potential. At this time we find features usually associated with a double layer,[23,29] in this case one moving with a velocity of approximately 0.02 v_{the} with v_{the} being the electron thermal velocity derived from the cathode temperature T_0. The analogy is best seen by concentrating on the part of phase space between the two vertical dashed lines. The important feature is that the free ions moving in the negative direction towards the cathode are some that have been reflected by the positive potential at the end plate. The trapped electron component is in reality a "blob" of electrons oscillating in a moving local potential maximum.[9] The double layer like structure dissolves when the source of reflected ions from the end plate is temporarily disrupted. The whole process repeats with the period of the instability.

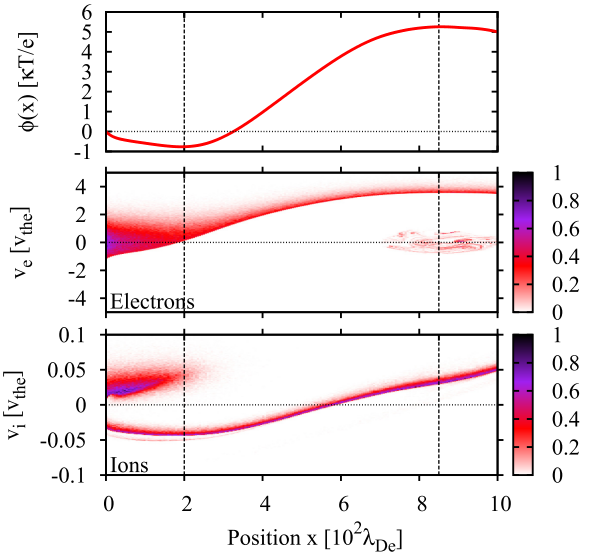

FIG. 4. Selected sample of spatial potential variation together with corresponding electron and ion phase spaces, illustrating transient double layer like features. The time is $t = 1270.47\,\omega_{pi}^{-1}$, i.e., a late time when the plasma has settled in a steady oscillatory state.

For completeness we show in Fig. 5 the space-time variation of the electrostatic potential and the corresponding net plasma current variation. The slope of the slanting shaded area in both figures gives a characteristic propagation velocity that corresponds to the velocity of the double layer like feature in Fig. 4.

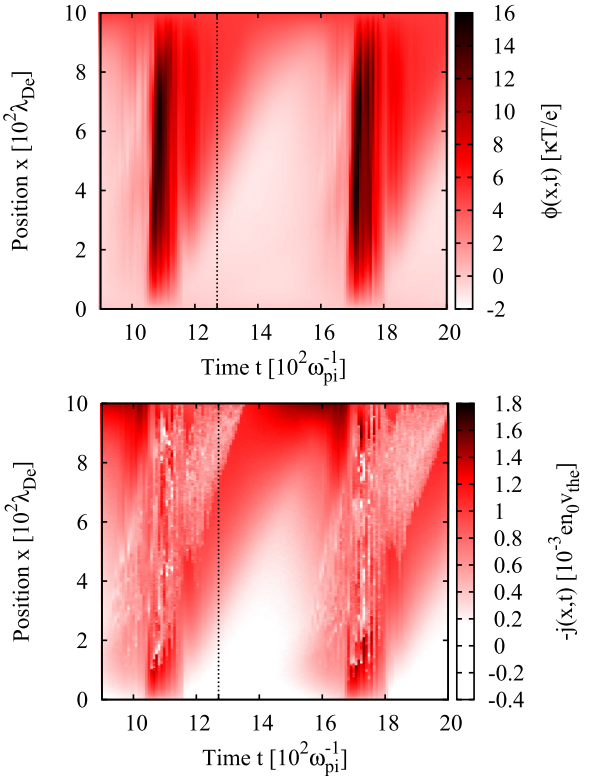

FIG. 5. Selected time interval of unstable diode oscillations. The top figure shows the space-time variation of the electrostatic potential, the lower figure shows the corresponding net plasma current variation. The vertical dashed line shows the time for the phase-space presentation shown in Fig. 4. In both cases the cathode is at the bottom of the figure.

Video 1 (Fig. 2) shows the full temporal evolution of electron and ion phase spaces. The formation and propagation of the transient double layer can be observed, in particular. From Fig. 1 we note a locally enhanced high frequency noise component at the negative extremum of the plasma current. Inspection of Video 1 (Fig. 2) demonstrates that this noise is due to a localized irregular "blob" of electrons trapped near a local potential maximum. The oscillations of these trapped electrons in their local, approximately parabolic, potential well gives rise to the observed noise. The details in the dynamics of the trapped electron population will be susceptible to collisions as discussed in Sec. VI.

As a test, we monitored the total number of simulation particles in the system during the simulations. This number was pulsating with the periodicity of the oscillations due to the modulated losses, but with constant end-plate potential we saw no systematically decreasing or increasing trend in the particle number, when averaged over one oscillation period.

IV. THE VAN DER POL MODEL

A standard and widely used analytical model for studying the nonlinear properties of driven linearly unstable systems is the van der Pol model

$$\frac{d^2}{dt^2}\xi - (\alpha - \beta\xi^2)\frac{d}{dt}\xi + \omega_0^2\xi = A\omega_0^2 \sin(\omega_e t), \qquad (4)$$

where we included a harmonic forcing. The coefficients $\alpha > 0$ and $\beta > 0$ refer to the linear growth phase and the nonlinear saturation, respectively, while ω_0 is the natural frequency of the oscillator and A is the amplitude of the forcing term. The variable ξ denotes any quantity of physical interest; in most of the present study it will be taken to be the current through the system. The right hand side of Eq. (4) can be made more general, but the form used here is the one found most often. The form Eq. (4) can be simplified by introducing a normalized time $\tau = t\omega_0$ and a normalized amplitude $\eta = \xi/\xi_0$ with $\xi_0 \equiv \sqrt{\alpha/\beta}$ to obtain $d^2\eta/dt^2 - \epsilon(1-\eta^2)d\eta/dt + \eta = A\sin(\tau\omega_e/\omega_0)/\xi_0$ where $\epsilon = \alpha/\omega_0$.

The results of Fig. 1 indicate that the onset of the oscillations is sudden: they reach maximum amplitude within approximately one period of oscillations. This feature was confirmed also by other detailed simulations where the end plate potential was changed from being below to being above threshold by a step function. The van der Pol model therefore needs a growth rate comparable to the frequency. In Fig. 6 we show results for diode simulation data (shown with full line) and numerical solutions of the van der Pol equation (4) with $A = 0$ and parameters adjusted to $\alpha/\omega_0 = 0.1$ for optimum fit. The parameters are chosen to give the best fit to the numerical observations. The results summarized Fig. 6 indicate that the van der Pol equation is able to give a very convincing representation of the performance of the steady state oscillations of the plasma diode without forcing. We have analyzed a wide parameter range giving consistent results.

In Fig. 7 we show numerical solutions of the normalized van der Pol equation. Two cases are considered: one (top figure) by applying a chirped frequency with constant amplitude as forcing on the right hand side, and one (bottom figure) with a

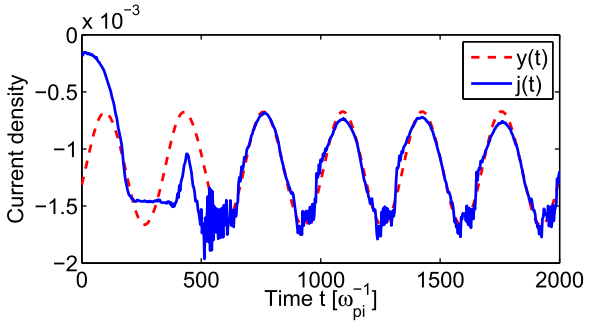

FIG. 6. Solution of the normalized van der Pol equation (dashed line) with parameters fitted to the data from the diode simulations (full line). Equation (4) is here solved without forcing with $\alpha/\omega_0 = 0.1$. The simulation data for the plasma current are obtained with a constant positive end plate bias.

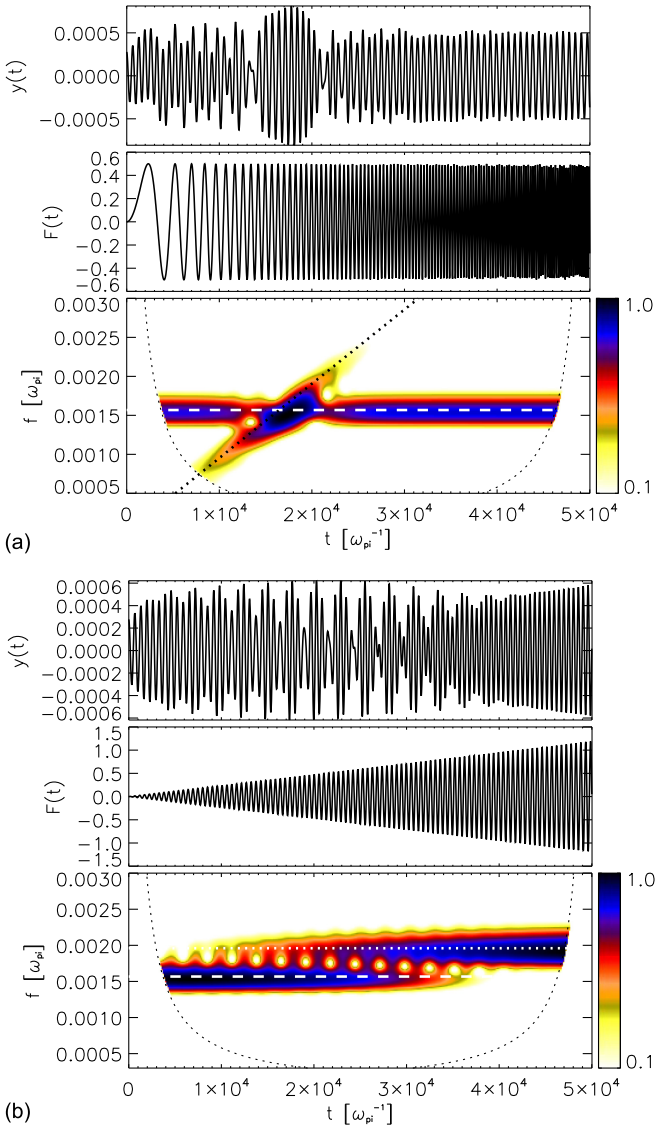

FIG. 7. Top figure: numerical solution of the van der Pol equation (4) in its normalized form with $\epsilon = 0.1$, here applying a chirped frequency with constant amplitude as forcing on the right hand side. The dotted oblique line gives the local frequency of the applied forcing. Bottom figure: forcing with constant frequency but with a linearly increasing amplitude. The wavelet transform of the resulting signal is shown in both cases.

constant frequency (here taken to be larger than f_0) but with a linearly increasing amplitude. The wavelet transform of the resulting signal is shown for both cases. The conspicuous feature of the solution with chirped frequency is the "frequency pulling" characteristic of the van der Pol equation. This is seen as the tilted frequency response in the local wavelet transform in the lower panel of Fig. 7(a), where the frequency of the oscillation response becomes synchronized with the applied signal. An increase in amplitude of the forcing increases the time interval where the synchronization can be observed. We note the absence of harmonic interactions in the numerical solutions. The constant frequency solutions illustrate how the natural mode of oscillation is stabilized (that is the frequency shifted or synchronized with the external forcing) for a sufficiently large amplitude of the excitation.

V. PERTURBATIONS OF THE DIODE

Mathematically, the question of forcing within the van der Pol equation is simple: an additional term is inserted on the right hand side as shown in Eq. (4). For a physical diode, a forcing can be applied in several ways, not necessarily equivalent.

The diode can be forced by applying a signal either to the end plate or at some internal position in the system. The two cases will be distinguished here, external end plate and internal forcings. One of the aims will be to analyze two of the characteristic features of the van der Pol model, synchronization and frequency pulling.[11,12,28] These features can be demonstrated most easily by a wavelet analysis of the data.[30]

We made two series of simulations, using two different forcing signals: one with a fixed frequency but varying amplitude and one with fixed amplitude but with "chirped" frequency.

The simplest form of external excitation (both in laboratory and in simulations) consists of applying an external signal to the cold end plate of the diode. The plasma diode can also be forced internally. In a Q-machine this forcing is usually achieved by immersing a fine-meshed grid in the plasma and then applying some time-varying signal to this grid. The operation of such a grid and its interaction with the plasma has been subject to some controversy,[6,31] where one model assumes that the local charge distribution is important and another that the modulated ion absorption is the dominant excitation mechanism. We start by discussion the two latter cases.

A. Oscillating localized electric field

We considered a model where externally controlled charges were introduced at two nearby grid-points (here separated by $10\lambda_D$) with opposite polarity. These charges came in addition to the ones arriving at the grid-points from the surrounding plasma. The excitation mechanism is here due to particle acceleration by the local electric field between the two charged grid-points. This form of excitation corresponds to a velocity modulation rather than a density modulation. We found that internal excitation by this method was indeed possible, but the charges applied had to be very large. The results were inconclusive and are not reported here. The excitation mechanism using an oscillating electric dipole was important for the early discussions of analytical studies of linear ion acoustic Landau damping.[31] As a practical method of wave excitation it seems to have little value in comparison to the model based on a grid giving a modulated particle absorption to be discussed in Sec. V B.

B. Locally modulated ion absorption

In Fig. 8 we show results from numerical simulations with internal excitation by modulated particle absorption, here by a signal chirped in frequency with constant oscillation amplitude. Ions are absorbed with a probability independent of their velocity. This form of excitation corresponds to the generally accepted model for wave excitation by a grid immersed perpendicular to the magnetized plasma column in a Q-machine.[6,28,32] For the case illustrated in Fig. 8 the absorption is strong, varying harmonically in the range 0%–70% at a position $3\mathcal{L}/7$, that is, the absorbing "grid" is at the position $x/\lambda_{De} \approx 430$. This method of excitation captures the essential part of grid excitation in, for instance, Q-machines at low applied frequencies. A missing element in the simulations is the electric fields being set up by the potential difference between the grid and the plasma vessel when a time varying potential is applied to the grid.

We note the distinct frequency pulling signature when the chirped frequency comes near the natural nonlinear oscillation frequency of the diode, i.e., in the frequency interval $f_0/2 - 3f_0/2$, approximately, where f_0 is the natural oscillation frequency. At the same time we note also an enhancement of the second harmonic, a feature not accounted for by the van der Pol equation. Even more interesting is the strong frequency pulling of the basic oscillator frequency observed

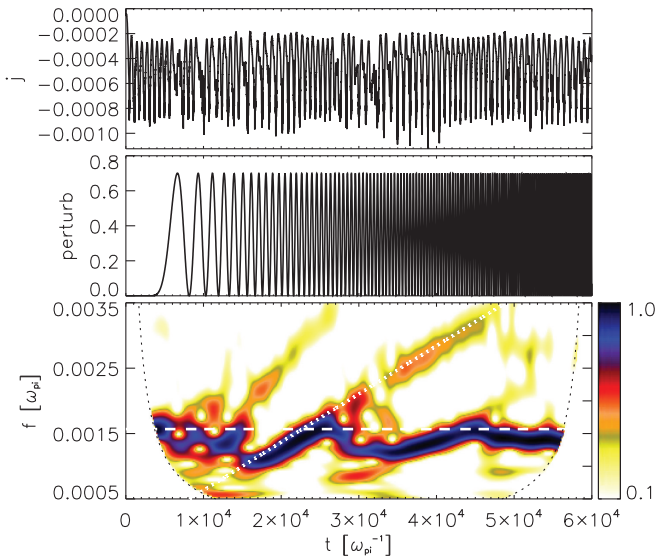

FIG. 8. Numerical simulations with internal excitation by modulated particle absorption, here by a chirped signal with constant amplitude. The top panel show the net current through the diode, the middle panel shows the time-varying absorption at a reference position, here at $x = (3/7)\mathcal{L}$, while the lower panel shows the wavelet transform of the time varying current. The horizontal dashed line in the lower panel shows the natural oscillation of the free oscillator for the given DC end plate bias, while the dotted oblique line gives the local frequency of the applied forcing.

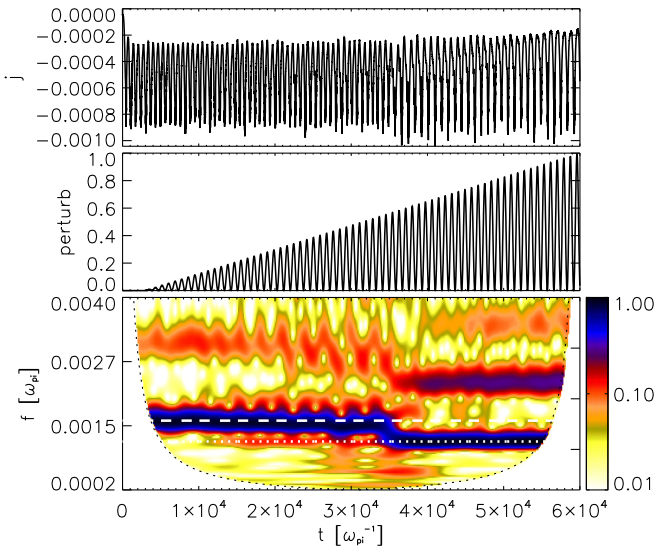

FIG. 9. Numerical simulations with internal excitation by modulated particle absorption, here by a signal with constant frequency somewhat below the natural oscillation frequency given by the dashed line (see also Video 2 (Fig. 10)). The amplitude of the oscillations increases from zero level with full ion transmission to 100% modulation where the ion transmission oscillates between 0 and 100%. The top panel show the net current through the diode, the middle panel shows the time-varying absorption at a reference position at $x = (3/7)\mathcal{L}$, while the lower panel shows the wavelet transform of the time varying current. The dashed line in the lower panel shows the natural oscillation frequency of the free oscillator for the given end plate bias, while the dotted line gives the frequency of the applied forcing.

when the applied frequency is in the range $3f_0/2 - 2f_0$. In this latter range, the strong oscillation has a frequency close to half the applied frequency. At reduced excitation amplitudes we will, however, see perturbations of the diode oscillations also at half oscillator frequency. These effects are masked in Fig. 8 by the frequency pulling which becomes effective already at frequencies close to half of the free oscillation frequency.

At time intervals when the applied frequency lies near the natural oscillation frequency f_0 and $3f_0/2$, we note excitation also of $f_0/2$. A weak signature of this frequency is seen also when the applied frequency is near $2f_0$.

We have tried different positions of the excitation point. Taking, for instance, $5\mathcal{L}/7$ we recover all the basic features of Fig. 8, but now with a reduced amplitude. Our conclusion from these and similar results is that the strongest excitation is found when the perturbation is close to the cathode. In this case the induced perturbation has the longest interaction distance with the ion flow before it reaches the end plate.

In Fig. 9 we show results where the frequency of the ion absorption is constant, but the temporally varying absorption ratio increases from 0 to 100% in the peak values. See also Video 2 (Fig. 10). The applied frequency is here below the natural frequency of the diode oscillations. For the present choice of parameters we find a transition in the oscillator characteristics at an absorption level of approximately 60%. Here the natural diode oscillations disappear completely, while we find a perfect locking to the applied frequency. At

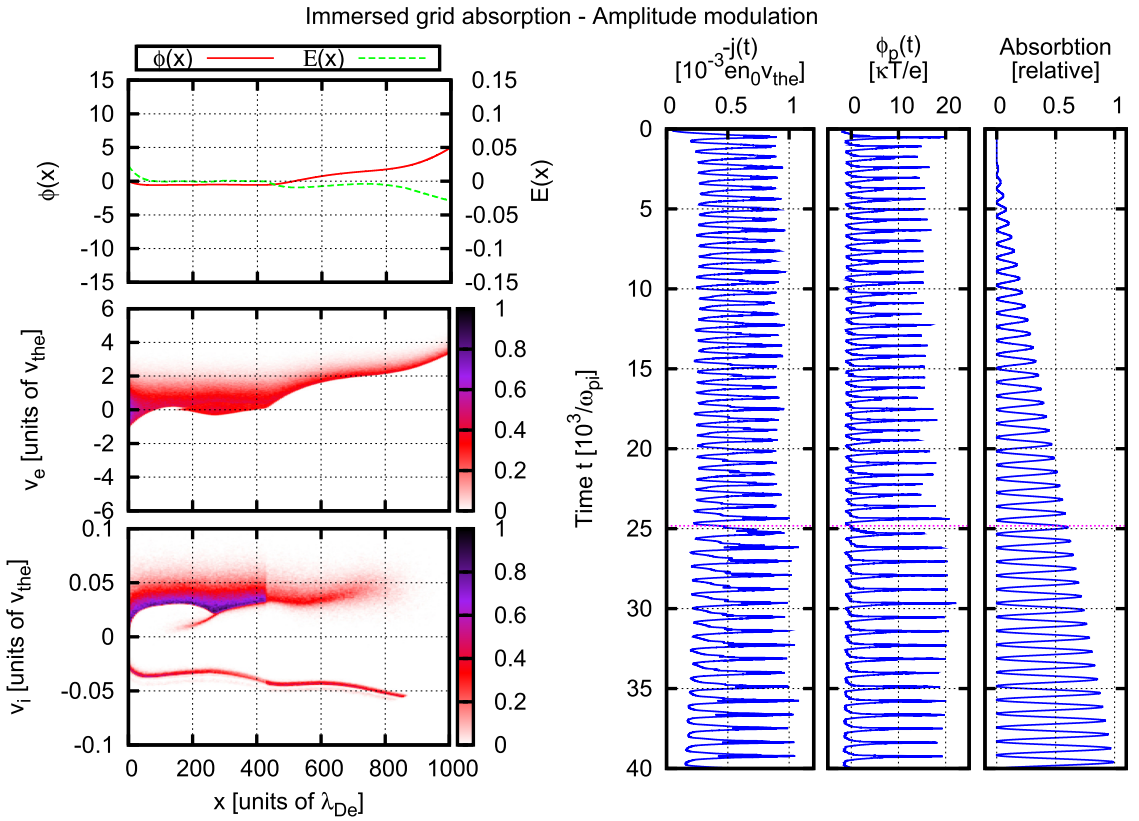

FIG. 10. Summary figure for Video 2, showing also the phase space dynamics. The simulations model an absorbing grid at position $x = 430\lambda_D$ where the time varying relative absorption is shown in the third frame to the right. See Fig. 2 for a detailed description of the set-up (enhanced online) [URL: http://dx.doi.org/10.1063/1.4747620.2].

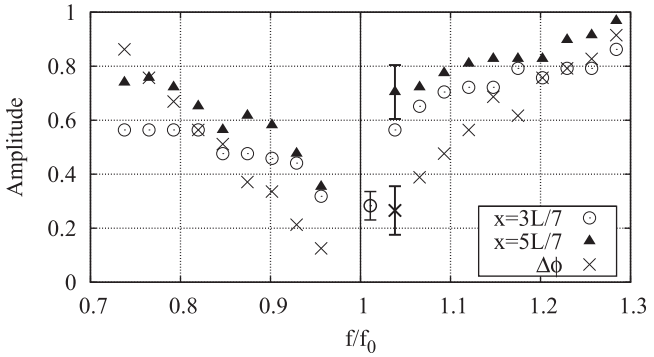

FIG. 11. Variation of the stabilizing amplitude with applied frequency. The error bar shown is representative for all open circles. Open circles correspond to the excitation applied at a position $3\mathcal{L}/7$, triangles to a position $5\mathcal{L}/7$. The error bar for the filled triangle represents the maximum uncertainty for those symbols. The figure also shows results (with $\times$-signs and a representative error bar) for the case where a signal is applied to the end plate.

the same time we find a very strong second harmonic enhancement, even the third harmonic becomes noticeable here. Prior to the onset of the synchronization we note a strong modulation of the free oscillator frequency and, in particular, also its second harmonic.

Consistent with the properties of the van der Pol model, we note that for a certain applied amplitude the free oscillation at frequency f_0 is quenched or stabilized, see again Video 2 (Fig. 10) (it may be confusing to use the term "stabilization" since the system is still oscillating at a large amplitude, but now at the applied frequency). The amplitude needed for this quenching depends on the applied frequency. We show in Fig. 11 results for the variation of this threshold amplitude for varying applied frequencies for two positions of the excitation. There is a noticeable asymmetry with respect to f/f_0, but qualitatively the results are similar to those expected from the van der Pol model, i.e., the threshold amplitude decreases as $|f - f_0|$ decreases, as also found experimentally.[32]

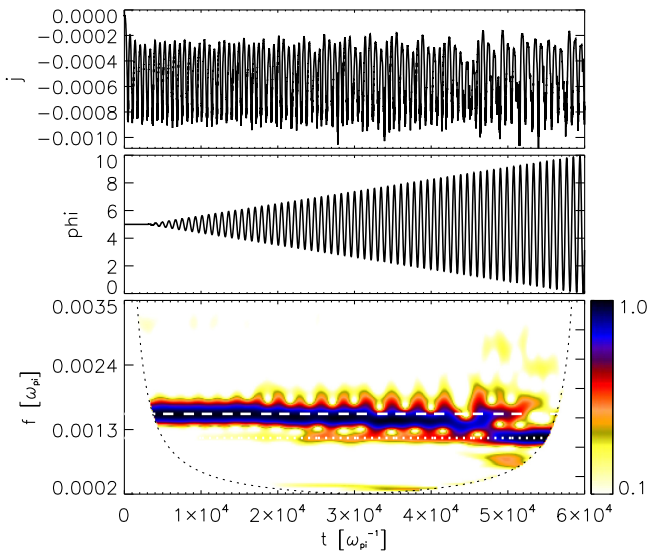

FIG. 12. The figure shows results for the case where a constant frequency with slowly increasing amplitude is applied to the positive end plate bias. The figure should be compared to Fig. 9.

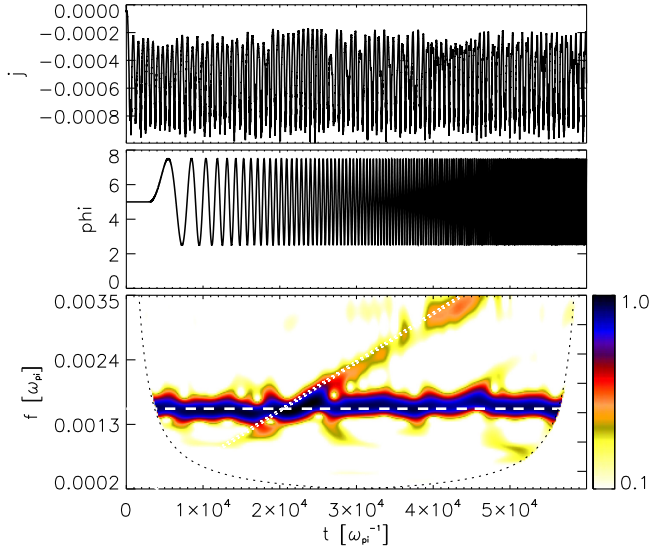

FIG. 13. The figure shows results for the case where a chirped frequency with constant amplitude is applied to the end plate. The figure should be compared to Fig. 8.

C. Modulated end plate bias

The external forcing can be applied also to the terminating end plate by adding a signal to the DC-bias. We used both amplitude and frequency modulations, as in Figs. 8 and 9. Illustrative results are shown Figs. 12 and 13 for a fixed frequency with linearly increasing amplitude and a fixed amplitude with chirped frequency, respectively. In many respects the results are similar to those found in Figs. 8 and 9, with one significant difference being in the harmonic content. We note the frequency pulling in Fig. 13 is very similar to that in Fig. 8, also when the local frequency approximates $2f_0$. Also, the frequency modulation in Fig. 12 is similar to what is seen in Fig. 9, but the signal at the second harmonic is completely absent. The feature near the frequency $f_0/2$ is absent in Fig. 13.

We show in Fig. 11 with crosses the normalized stabilizing amplitude A/A_0 where A_0 is the DC-bias applied to the end plate. For amplitudes $A > A_0$ the fundamental steady state oscillation amplitude is stabilized. We note also in this case a variation $A/A_0 \sim |f - f_0|$.

As a general feature we find that large amplitude oscillations have to be applied to the end plate in order to find observable effects: the amplitudes have to be significant fractions of the DC-bias. The necessary amplitudes depend on the DC-bias, provided the diode is conditioned to be in a fluctuating state.

VI. EFFECTS OF COLLISIONS

The foregoing analysis assumed ideal collisionless conditions. For realistic conditions we will often find that collisional effects cannot be ignored. Considering, for instance, a Q-machine operated with Caesium, which is a common practice, it is well known that the cross section for collisions of thermal electrons at relevant temperatures and neutral Caesium is particularly large.[33] Neutral Caesium originating from the neutral oven is found in abundance near the cathode. Also,

the ions will in this case experience collisions with the neutrals, where charge exchange collisions have the largest cross section, this type of interaction being resonant.[34]

We extended the analysis by considering also collisional interactions in the PIC-code.[20] Some basic features of our model are summarized in the Appendix. The numerical code offers an opportunity to introduce collisional effects for one species at a time: this is unphysical but offers an insight into the details in the process. We study ion neutral elastic collisions (IS), electron neutral elastic collisions (ES), and charge exchange ion collisions (CE). A summary of simulation results is presented in Fig. 14, where $\mathcal{L} = 10^3 \lambda_{De}$ as in Fig. 6. Two parameter regimes are analyzed: one where the scattering neutral gas temperature T_n equals the reference temperature T_0, while another case assumes $T_n = 0.15\,T_0$. In all cases we have taken the mean free path for collisions to be approximately 140 λ_D. For reference, we also include a result for the case where we have all collision processes activated: the mean free path for ion elastic and charge exchange collisions is here $460\lambda_D$ for both, giving an average ion mean free path of $230\lambda_D$, while the electron mean free path for elastic collision is $260\lambda_D$.

The characteristic diode oscillations are changed by the electron neutral collisions when we compare with the reference collisionless simulation also shown in Fig. 14. The high frequency oscillations due to the trapped electron component (see Video 1, Fig. 2) is quenched by the collisions, where we have the collisional mean free path to be shorter than the width of the potential well.[35] The form of the current signal becomes closer to the result obtained by the van der Pol model (see also Fig. 6). The sheath region near the emitting region at $x = 0$ is electron rich already without collisions,

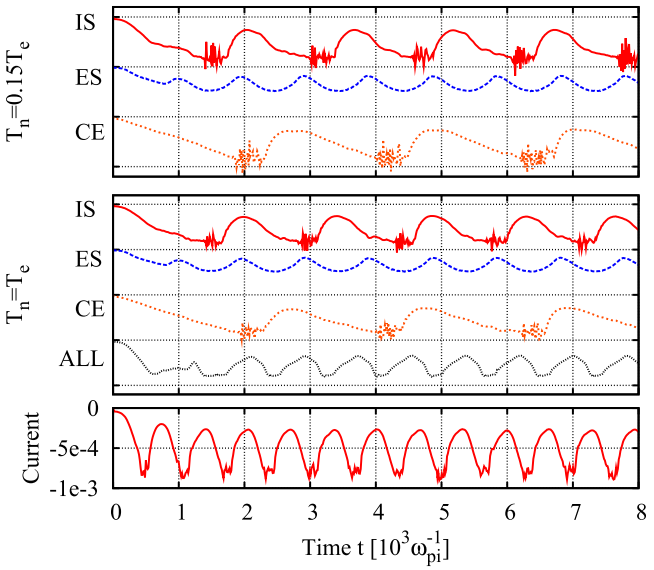

FIG. 14. Diode currents for selected collision processes. The bottom trace shows the reference calculations without collisions. The middle trace shows IS, ES, and CE, all assuming that the scattering neutral gas has the electron reference temperature at x = 0. The top frame shows results corresponding to the middle frame, but now with the scattering gas being colder, $T_n = 0.15\,T_0$. The trace denoted "ALL" represents a simulation where all collisions are activated simultaneously.

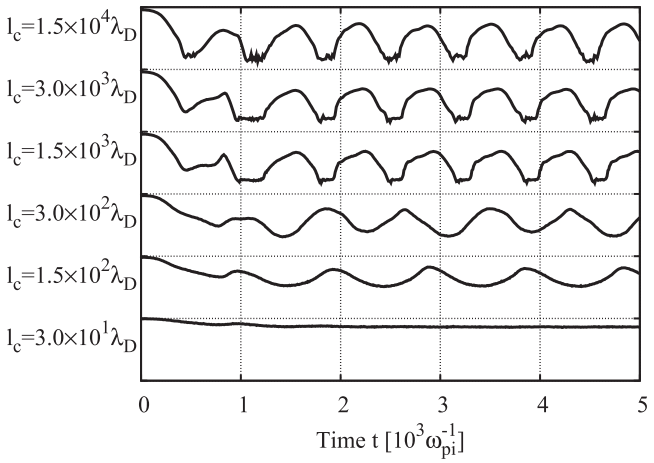

FIG. 15. Diode currents for different electron neutral collisions. The imposed collisional mean free path ℓ_c is indicated at each curve. The ions are here collisionless.

and an additional slowing down of the electrons due to the collisions is merely enhancing the local excess of electrons there. The temperature of the scattering neutrals has little effect in this context.

While Fig. 14 is a summary plot, we show in Fig. 15 the detail of the effect of elastic collisions of electrons and neutrals. As long as the collisional mean free path is longer than $\mathcal{L}$ as in the three top traces in Fig. 15, the collisions have modest effect, but as the collisions become more abundant, the frequency of the oscillations decreases slowly with decreasing collisional mean free path. At the same time the amplitude decreases to be almost indiscernible when the mean free path is approximately $\mathcal{L}/30$. At this stage the electron mobility is low, and the local electron density becomes large in front of the emitting surface. For the shortest mean free paths in Fig. 14, we observe the transient formation of an ion phase space vortex.[36,37] The life time of these vortices seems to increase with decreasing collisional mean free paths. If we decrease the collision mean free path even further, we find a new type of small amplitude oscillations with a frequency that is higher than seen in Fig. 14: these oscillations are due to the mobile ions.

Ion collisions are effective in modifying the diode; charge exchange collisions are more effective than elastic ion collisions. To gain some insight into the details of the elastic ion collision processes, we determined an estimate for the joint probability density $P(E_1, E_2)$, where E_1 is the ion energy at the beginning of a mean free collision path and E_2 the energy of the ion at the next collision time. The analysis does not discriminate the positions of the collisional ion. The marginal distributions $P(E_1)$ and $P(E_2)$ are obtained by projecting $P(E_1, E_2)$ on the E_1 and E_2 planes. We found that approximately we have $P(E_1, E_2) \approx P(E_1)P(E_2)$, indicating that to a good approximation we can assume E_1 and E_2 to be statistically independent. This means that the collective electric fields are just as effective as the elastic collisions in randomizing the ion energies. The main characteristics of the oscillations with significant charge exchange collisions (traces "CE" in Fig. 14) is a decrease in the oscillation period (for elastic

collisions, this has been observed also experimentally[2,38]), together with a distortion of the form of the oscillations, that becomes "saw-tooth" like. When all collisional effects are activated (see the trace labelled "ALL" in Fig. 14), we find that the saw-tooth feature is still there but now with a "tilt" to the opposite side, thus demonstrating that the temporal form of the oscillations is sensitive to the nature of the collisions. The results presented in Fig. 14 include the initial transient part of the oscillations: we note significant modifications also in this part when we compare with the reference collisionless case.

When the collisional charge exchange drag on the ions is large, we find the formation of a positive space charge layer near $x = 0$, and the diode oscillations are modified. Details in the propagation characteristics in the space-time varying potential found in Fig. 5 disappear. Charge exchange collisions are more effective than elastic collisions in slowing down the ions, and charge exchange collisions with a cold neutrals are more effective than similar collisions with warm neutrals. All these observations are consistent with the results summarized in Fig. 14. If we take the neutral gas temperature to be very low, we find that the ion component can develop two distinct populations[39]: one being the part accelerated through the potential drop at the sheath having not yet collided, and a part formed by the charge exchange collisions and appearing as a cold component with no drift velocity. In this case we can have a kinetic ion-ion instability developing.[40] This result has interest only for very low temperatures T_n and is not elaborated further here. For very high ion collision rates the ion mobility becomes low, but the oscillations can be maintained by the electron dynamics alone, as for a Pierce diode[41] provided the conditions on geometry and end-plate bias are fulfilled. For such low ion mobilities, the average ion distribution will be non-uniform.

The almost linear scaling between oscillation period and the length of the system (shown in Fig. 3) remains valid also when we have significant amounts of collisions, but the frequency is now noticeably reduced and we have $f_0 \approx C_s/2\mathcal{L}$; see results given by squares in Fig. 3, where a full line gives the sound speed, and dotted line is the best fit to the data (squares). The difference is minute.

In Video 3 (see Fig. 16) we show the space-time variation of the diode, giving the potential as well as the phase-space information for the case where $T_n = 0.15\,T_0$. We initiate the simulation with no collisions and let the mean free path be slowly decreasing until it reaches a value slightly smaller than the one used for Fig. 14. We have $\ell_c \sim 1/t$ so that the average collision frequency becomes approximately proportional to time. The effects of charge exchange collisions begin to be noticeable when the collisional mean free path is approximately $\mathcal{L}/2$. The formation of the cold ion population due to the charge exchange processes is clearly seen in ion phase space. The results should be compared to the free oscillations shown in Video 1 (Fig. 2). Note that the number of ions reflected at the end plate is strongly reduced for the case with charge exchange collisions. The

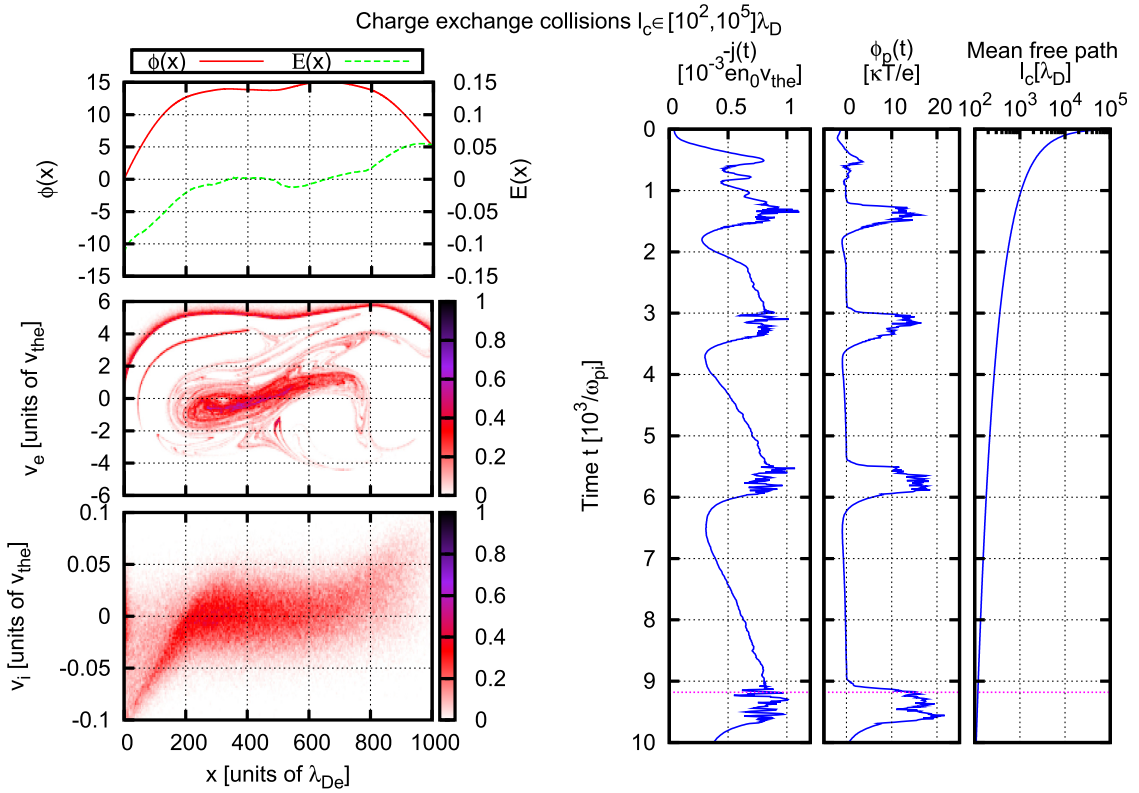

FIG. 16. Summary figure for Video 3, showing also the phase space dynamics. The simulations model the case where the ion charge exchange collisional mean free path decreases with time as shown in the third frame to the right. See Fig. 2 for a detailed description of the set-up (enhanced online) [URL: http://dx.doi.org/10.1063/1.4747620.3].

propagating double layer structure is not significant with charge exchange collisions, but the basic characteristics of the diode oscillations remain, albeit with reduced frequency and distorted temporal form of the oscillations. In Video 3 (Fig. 16) we show in the rightmost panel also the electrostatic potential as detected at a position $x = \mathcal{L}/2$. At this position we find localized potential enhancements with long quiescent time intervals in between, where all of the potential drop in the diode is found at the end sheath.

Also with collisions included, we find that the diode retains the basic properties of a van der Pol oscillator. For illustration we show in Fig. 17 the diode performance with external forcing of a diode where the ions have charge exchange collisions where $\ell_c = 150\lambda_D$. The top trace shows the diode current, the next frame is the potential applied to the end-plate. The third frame from the top gives the plasma potential in the central position of the diode, while the bottom frame gives the wavelet transform of the current. A dashed line gives for reference the natural frequency of the diode without collisions and constant positive end-plate potential. When the externally applied frequency is near the collisional diode frequency, we observe the frequency pulling in the wavelet transform of the diode current. When the difference between the natural and applied frequencies is large, we find that the oscillations return to the frequency of the constant bias diode. These low frequency oscillations modulate the high frequency applied signal resulting in bursts or "packets" of high frequency signals, most clearly observed in the wavelet transform. We note a similarity with the corresponding results in Fig. 13 for a collisionless diode.

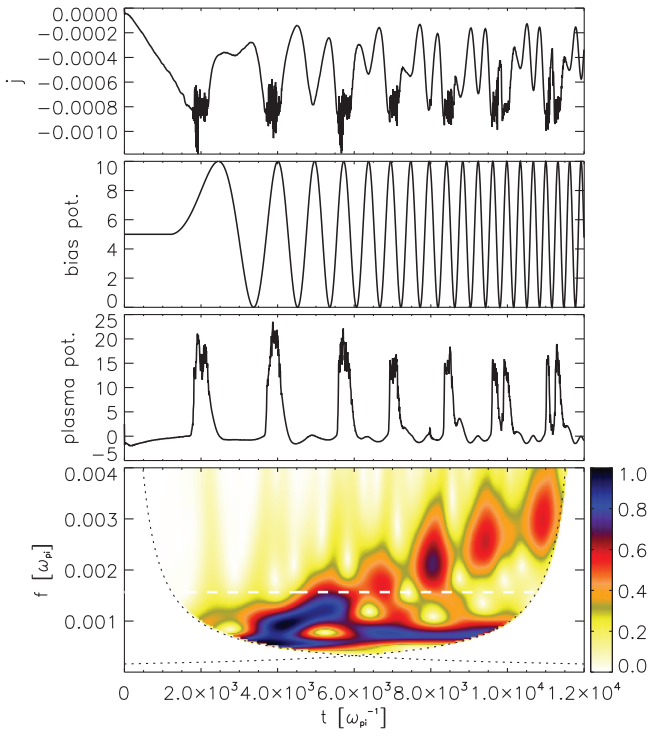

FIG. 17. External forcing of a diode with ions have charge exchange collisions where $\ell_c = 150\lambda_D$. The top trace shows the diode current, the next frame is the potential applied to the end-plate (see also Fig. 13). The third frame from the top gives the plasma potential in the central position of the diode, while the bottom frame gives the wavelet transform of the current. A dashed line gives for reference the natural frequency of the diode without collisions and constant positive end-plate potential.

VII. DISCUSSIONS

In the present study we analyzed the properties of a simple plasma diode with emphasis on the conditions with forcings applied either to the boundary of the plasma or internally by introducing either variable test charges or particle absorption. We compared the properties of the diode with solutions of the van der Pol equation. It was found that for the unperturbed oscillation, i.e., without applied forcing, a very good agreement could be found. Extending the analysis to the externally forced diode we found qualitative agreement in the sense that some basic features of the van der Pol equation could be recovered, but here it was important to specify the means of external excitation. The most effective excitation turned out to be one corresponding to an absorbing grid immersed in the plasma column. Incidentally, this method was used by some of the early investigations of the diode performance.[28] Velocity modulation by a localized electric field had a much smaller effect in comparison.

Another method of diode perturbation consists of applying a variable, externally controlled, potential to the end plate. We analyzed also this method and found that in this case elements of the results from a perturbed van der Pol equation could be recovered. It was, however, necessary to apply external amplitudes comparable to the DC bias, an observation which is after all also intuitively reasonable. This latter method of excitation is the one that comes closest to giving results similar to those found by solving the van der Pol equation with external forcing. We find, however, the similarities of the results to be more interesting than the differences: the two very different methods of excitation both reproduce the periodic pulling and mode stabilization features found in the van der Pol model.

The excitation obtained by modulating the end plate bias corresponds to applying an ideal voltage generator,[20] i.e., one that maintains a potential irrespective of the load. The case where the end plate voltage is modulated can be modeled by a dc-generator in series with a variable generator, both elements considered ideal. The alternative ideal generator used in lumped electrical circuits, the ideal current generator (one that maintains the current irrespective of the load), is not readily realized experimentally and therefore not studied here. As a first approximation it can be argued that the modulation of the ion flux passing a reference position as described in Sec. V B is equivalent to a current modulation. Such a model can be taken only as an approximation, however, since the efficiency depends on the position of the excitation along the axis of the device as evidenced by Fig. 11.

The most significant difference between the diode simulations and the numerical solutions for the van der Pol equation lies in the second and third harmonic generation. These were much more significant in the numerical simulations of the diode, and we conclude that the nonlinear term in the van der Pol model has to be elaborated for a better agreement and

found also that a simple addition of terms with exponents exceeding 2 is not sufficient. We found numerical confirmations also of experimentally observed propagating double layers.[23] Details concerning the ion population are not readily revealed experimentally, and numerical simulations like those presented here are necessary for a complete understanding. The internal modulations destroy the propagating double layer, and the stabilization of the van der Pol oscillations for that case is in part due to this effect. When the applied frequency is very high compared to the natural frequency, the perturbation reduces to a local modulation of the plasma density, where the oscillating diode returns approximately to its original state with a DC-bias.

In all cases we found that large forcing amplitudes have to be applied to the system in order to recover solutions resembling those characterizing a van der Pol oscillator. We tried various modifications of the basic van der Pol equation to make its solutions closer to observations but found that minor modifications are insufficient. Terms containing $d\xi/dt$ as well as ξ in the bracket of the nonlinear term of (4) were tried.

The effect of collisions was discussed in Sec. VI. Several types of collisions were studied. We found that charge exchange collisions were particularly effective in modifying the oscillation characteristics of the diode, with results summarized in Figs. 3 and 14. Charge exchange collisions usually have the largest cross sections and are physically the most relevant. The most important observation regarding the oscillation characteristics of the diode with collisions seem to be a pronounced reduction in oscillation frequency. Also, a change in shape of the signal is noted: the current becomes more "saw-tooth like," with an increased harmonic content with collisional ions, while electron collisions on the other hand give smoother signals, with less harmonic content. For the collisionless diode we find that the growth of the large amplitude perturbation begins at the sheath near the end plate, and progresses rapidly into the main plasma (see Video 1 (Fig. 2)). For the collisional diode, with the parameters studied here, the perturbation begins at the plasma emitting plate to propagate rapidly into the main plasma, see Video 3 (Fig. 16). Our three videos offer detailed insight into the phase space dynamics of ions as well as electrons. The general space-time characteristics of the oscillations are changed, e.g., details in the double layer like structure shown in Fig. 4 are lost.

ACKNOWLEDGMENTS

The work was supported in part by a grant from the Norwegian National Science Foundation. We thank Dr. Wojciech Miloch for his interest and for many valuable discussions on numerical problems.

APPENDIX: DETAILS OF THE COLLISION ALGORITHM

The numerical collision model developed for the present study is based on a Monte Carlo collision (MCC) model for PIC simulation codes and is directly based upon previous works.[42,43] While traditional collision models[44,45] calculate the time between collisions for each particle, the MCC-PIC package generalizes these calculations to allow for more efficient algorithms.

The collision algorithm is based on the null-collision methodology. Instead of entering the rather time-consuming evaluation of cross section $\sigma(E)$ or equivalently collision frequency $\nu(E)$ for each simulation particle at each time step, a maximum collision frequency $\nu_{\max}$ is introduced for each particle species

$$\nu_{\max} \equiv \max_E \Big(\sum_s \nu_s(E) \Big), \tag{A1}$$

where $\nu_s(E)$ is the collision frequency of type s for the given specie. Potential candidates for collision events during the time interval Δt are now draw with probability $P = 1 - \exp(-\nu_{\max}\Delta t)$. For these candidates *only* the exact evaluation of $\nu(E)$ is performed. A fraction $\nu(E)/\nu_{\max}$ of the potential candidates drawn are then subjected to an actual collision event. The remaining fraction suffer a "null-collision," that is they avoid collisions in the given time interval Δt.

The current model allows for both elastic and inelastic scattering and charge exchange collisions, for any arbitrary combination of particle species, with input parameters as cross sections, scattering angles, and VDF's of the target species given. Cross section and scattering angles are generally given as functions of kinetic energy in a centre-of-mass reference system.

The present study is restricted to constant cross sections and isotropic scattering. Realistic scattering cross sections that vary with energy and which may differ significantly from one species to another can be readily introduced. For the illustration intended with the present analysis we find that constant cross sections and, thereby, constant mean free paths will suffice. Taking the cross section to be constant, independent of energy, allows us to use a constant mean free path for all particles.

[1]R. W. Motley, *Q Machines* (Academic, New York, 1975).
[2]T. Klinger, F. Greiner, A. Rohde, and A. Piel, "Nonlinear dynamical behavior of thermionic low-pressure discharges. 2. Experimental," Phys. Plasmas **2**, 1822–1836 (1995).
[3]I. Langmuir and K. H. Kingdon, "Thermionic effects caused by vapors of alkali metals," Proc. R. Phys. Soc. Ser. A **107**, 61–79 (1925).
[4]H. B. Michaelson, "The work function of the elements and its periodicity," J. Appl. Phys. **48**, 4729–4733 (1977).
[5]F. Bauer and H. Schamel, "Spatiotemporal structures in collisionless electrostatic plasmas," Physica D **54**, 235–252 (1992).
[6]S. Kuhn, "Determination of axial steady-state potential distributions in collisionless single-ended Q-machines," Plasma Phys. **21**, 613–626 (1979).
[7]T. L. Crystal, P. C. Gray, W. S. Lawson, C. K. Birdsall, and S. Kuhn, "Trapped-electron effects on time-independent negative-bias states of a collisionless single-emitter plasma-device-theory and simulation," Phys. Fluids B-Plasma Phys. **3**, 244–254 (1991).
[8]T. Seo, J. C. I. Kim, and S. J. Hahn, "Nonlinear dynamical behaviors in a magnetized plasma diode system," J. Phys. Soc. Jpn. **80**, 034501 (2011).
[9]V. I. Kuznetsov, A. Ya. Énder, and S. Kuhn, "Collisionless self-consistent trapping of electrons into a nonstationary potential well: Dynamics of trapped electrons," Tech. Phys. **51**, 1257–1268 (2006).
[10]V. I. Babanin, I. N. Kolyshkin, V. I. Kuznetsov, A. S. Mustafaev, V. I. Sitnov, and A. Y. Énder, "Optimization of a Knudsen Cs-Ba thermionic converter," Sov. Phys. Tech. Phys. **223**, 444–766 (1978); "Optimization of a Knudsen Cs-Ba thermionic converter," Z. Tech. Fiz. **48**, 754–766 (1978).
[11]T. Gyergyek, M. Čerček, and M. Stanojević, "Experimental evidence of periodic pulling in a weakly magnetized discharge plasma column," Contrib. Plasma Phys. **37**, 399–416 (1997).

[12]H. Lashinsky, "Turbulence in Fluids and Plasmas," Microwave Research Institute Symposia Series, Vol. **18** (Polytechnic, Polytechnic Institute of Brooklyn, NY, 1969).
[13]T. Klinger, F. Greiner, A. Rohde, A. Piel, and M. E. Koepke, "van der Pol behavior of relaxation oscillations in a periodically driven thermionic discharge," Phys. Rev. E **52**, 4316–4327 (1995).
[14]K. H. Pae and S. J. Hahn, "Self-oscillation and chaos in positive-bias plasma diodes," J. Phys. Soc. Jpn. **71**, 2169–2173 (2002).
[15]A. Piel, F. Greiner, T. Klinger, N. Krahnstover, and T. Mausbach, "Chaos and chaos control in plasmas," Phys. Scr. T **84**, 128–131 (2000).
[16]A. Ya. Énder, H. Kolinsky, V. I. Kuznetsov, and H. Schamel, "Collective diode dynamics: An analytical approach," Phys. Rep. **328**, 1–72 (2000).
[17]V. I. Kuznetsov, A. Ya. Énder, H. Schamel, and P. V. Akimov, "Switching of nonneutral plasma diodes. I. Analytic theory," Phys. Plasmas **11**, 3212 (2004).
[18]V. I. Kuznetsov, A. Ya. Énder, H. Schamel, and P. V. Akimov, "Switching of nonneutral plasma diodes. II. Numerical results," Phys. Plasmas **11**, 3224 (2004).
[19]Y. A. Énder, V. I. Kuznetsov, and H. Schamel, "Theory and application of plasma diode equilibria with beam electrons and a fixed particle background of negative charge," EPJ.-Appl. Phys. **49**, 11002 (2010).
[20]F. Greiner, T. Klinger, and A. Piel, "Nonlinear dynamical behavior of thermionic low-pressure discharges. 1. Simulation," Phys. Plasmas **2**, 1810–1821 (1995).
[21]F. F. Chen, *Introduction to Plasma Physics and Controlled Fusion*, 2 ed. (Plenum, New York, 1984), Vol. 1.
[22]M. A. Lieberman and A. J. Lichtenberg, *Principles of Plasma Discharges and Materials Processing* (John Wiley & Sons, Inc., New York, 1994).
[23]S. Iizuka, P. Michelsen, J. J. Rasmussen, R. Schrittwieser, R. Hatakeyama, K. Saeki, and N. Sato, "Dynamics of a potential barrier formed on the tail of a moving double-layer in a collisionless plasma," Phys. Rev. Lett. **48**, 145–148 (1982).
[24]T. Klinger and A. Piel, "Investigations of attractors arising from the interaction of drift waves and potential relaxation instabilities," Phys. Fluids B **4**, 3990–3995 (1992).
[25]C. K. Birdsall and A. B. Langdon, *Plasma Physics via Computer Simulation* (McGraw-Hill, New York, 1985).
[26]P. Burger, "Theory of large-amplitude oscillations in 1-dimensional low-pressure cesium thermionic converter," J. Appl. Phys. **36**, 1938–1943 (1965).
[27]J. E. Crow, P. L. Auer, and J. E. Allen, "Expansion of a plasma into a vacuum," J. Plasma Phys. **14**, 65–76 (1975).
[28]P. Michelsen, H. L. Pécseli, J. J. Rasmussen, and R. Schrittwieser, "Current-driven, ion-acoustic instability in a collisionless plasma," Plasma Phys. Controlled Fusion **21**, 61–73 (1979).
[29]H. Schamel, "Electron holes, ion holes and double layers," Phys. Rep. **140**, 161–191 (1986).
[30]S. Mallat, *A Wavelet Tour of Signal Processing* (Academic, California, 1998).
[31]R. W. Gould, "Excitation of ion-acoustic waves," Phys. Rev. **136**, A991–A997 (1964).
[32]P. Michelsen and H. L. Pécseli, "Propagation of density perturbations in a collisionless Q-machine plasma," Phys. Fluids **16**, 221–225 (1973).
[33]Y. Itikawa, "Effective collision frequency of electrons in gases," Phys. Fluids **16**, 831–835 (1973).
[34]S. A. Andersen, V. O. Jensen, and P. Michelsen, "Charge-exchange cross-sections measured at low energies in Q machines," Rev. Sci. Instrum. **43**, 945–947 (1972).
[35]R. Ya. Kucherov, Z. A. Oganezov, L. S. Timoshenko, and V. K. Tskhakaya, "Electric field distribution in a Knudsen plasma," Sov. J. Plasma Phys. **15**, 766–771 (1989).
[36]H. L. Pécseli, R. Armstrong, and J. Trulsen, "Experimental observation of ion phase-space vortices," Phys. Lett. A **81**, 386–390 (1981).
[37]H. L. Pécseli, J. Trulsen, and R. Armstrong, "Formation of ion phase-space vortexes," Phys. Scr. **29**, 241–253 (1984).
[38]I. G. Gverdtsiteli, V. Ya. Karakhanov, E. A. Kashirskii, R. Ya. Kucherov, and Z. A. Oganezov, "Mechanism of flow oscillations in Knudsen cesium diode," Sov. Phys. Tech. Phys. **17**, 78–84 110 (1972); "Mechanism of flow oscillations in Knudsen cesium diode," Z. Tech. Fiz. **42**, 103–84 110 (1972).
[39]S. Børve, H. L. Pécseli, J. Trulsen, and S. Longo, "Kinetic instabilities associated with injection of a plasma beam into a neutral background," Phys. Scr. **T122**, 125–128 (2006).
[40]B. D. Fried and A. Y. Wong, "Stability limits for longitudinal waves in ion beam-plasma interaction," Phys. Fluids **9**, 1084–1089 (1966).
[41]J. R. Pierce, "Limiting stable current in electron beams in the presence of ions," J. Appl. Phys. **15**, 721–726 (1944).
[42]V. Vahedi and M. Surendra, "Monte Carlo collision model for the particle-in-cell method: Applications to argon and oxygen discharges," Comput. Phys. Commun. **87**, 179–198 (1995).
[43]C. K. Birdsall, "Particle-in-cell charged-particle simulations, plus Monte Carlo collisions with neutral atoms," IEEE Trans. Plasma Sci. **19**, 65–85 (1991).
[44]E. W. McDaniel, *Atomic Collisions: Electron and Photon Projectiles* (Wiley, New York, 1989).
[45]E. W. McDaniel, J. B. A. Mitchell, and M. E. Rudd, *Atomic Collisions: Heavy Particle Projectiles* (Wiley, New York, 1993).